Dynamics of phenyl-based polymer chains confined in thin layers

DISSERTATION

for the attainment of the academic degree

Bachelor of Science

at the
International Physics Study Program (IPSP) of the University of Leipzig

submitted by

Federico Porcelli
born on 16.03.2001 in Bisceglie

prepared in the
IPSP Leipzig

Supervised by
Dr. Martin Treß

Decision on the conferral of the bachelor degree dated 15.09.2024

Contents

0.1 Bibliography

Federico Porcelli

Dynamics of phenyl-based polymer chains confined in thin layers

Universität Leipzig, Dissertation

40 pages, 26 figures, 1 attachments

0.2 List of Abbreviations

Poly-TPD Poly([N,N'-diphenyl-N,N'-bis(4-tert-butylphenyl)-(1,1'-biphenyl)-4,4'-diamine]-alt-formaldehyde)

Poly-Bisphenol 4,4-Dihydroxydiphenyl-2,2-propane carbonate polymer

DF dielectric function

TPD triarylamine

HN Havriliak-Negami

EP electrode polarization

FA fluorene

OPV organic photovoltaic

OLED organic light-emitting diode

HTL hole transport layer

GPC gel permeation chromatography

BDS broadband dielectric spectroscopy

RMS root mean square

KK Kramers-Kronig

VFT Vogel-Fulcher-Tamann

DSC differential scanning calorimetry

GTT glass transition temperature (T_g)

PALS positron annihilation lifetime spectroscopy

RFOT Random First-Order Transition

ECNLE Elastically Collective Nonlinear Langevin Equation

Chapter 1

Introduction

In bulk polymers, physical properties such as heat capacity, thermal expansion coefficient, dielectric permittivity, and refractive index are well-defined and uniform. Studies of the glass transition in bulk polymers typically involve measuring changes in these parameters as a function of time or temperature. However, when polymers are confined to thin films, the situation changes significantly. The glassy dynamics near the interfaces alter, leading to variations in properties like dielectric permittivity, thermal expansion, heat capacity, and refractive index within the film. Unlike bulk materials, thin polymer films exhibit a heterogeneous response due to the complex interplay of these local variations. Consequently, measurements on thin films reflect a collective response that averages multiple local contributions.

The present work aims to illustrate how these contributions combine to produce the overall dielectric response of thin polymer films, particularly through broadband dielectric spectroscopy. The focus will be on two polymers in particular, namely Poly-TPD, studied for its superior charge transport properties in organic electronics, and P-Bisphenol, valued for its high thermal stability and mechanical strength in engineering applications.

Chapter 2

Theoretical Background

2.1 Basic Concepts

2.1.1 Maxwell's Equations

Maxwell's equations form the foundation of classical electromagnetism, describing how electric charges and currents produce electric and magnetic fields, as well as how those fields interact with each other and with matter. It is deemed worthwhile to quickly recall them:

1. **Gauß Theorem for Electricity:**
$$\nabla \cdot \mathbf{E} = \frac{\rho}{\epsilon_0} \tag{2.1}$$

2. **Gauß Theorem for Magnetism:**
$$\nabla \cdot \mathbf{B} = 0 \tag{2.2}$$

3. **Faraday's Law of Induction:**
$$\nabla \times \mathbf{E} = -\frac{\partial \mathbf{B}}{\partial t} \tag{2.3}$$

4. **Ampère's Law (with Maxwell's addition):**
$$\nabla \times \mathbf{B} = \mu_0 \mathbf{J} + \mu_0 \epsilon_0 \frac{\partial \mathbf{E}}{\partial t} \tag{2.4}$$

2.1.2 Electric Displacement Field

The electric displacement field **D** relates to the electric field **E** and the polarization **P** within a medium. It accounts for both free and bound charges in the material and is defined by the equation:

$$\mathbf{D} = \epsilon_0 \mathbf{E} + \mathbf{P} = \epsilon_0 \boldsymbol{\epsilon} \mathbf{E}$$

where ϵ_0 is the permittivity of free space, **E** is the electric field, **P** is the polarization vector (i.e. dipole moment per unit volume of the material), and $\boldsymbol{\epsilon}$ represents the dielectric function (DF) and is generally a tensor of rank 2 because of the non-required collinearity between **D** and **E**.

2.1.3 Complex Dielectric Function

In most instances though, $\boldsymbol{\epsilon}$ will be treated as a complex (scalar) function $\epsilon^*(\omega)$, which varies with frequency due to the contributions of different oscillators in the analyzed materials. Namely it's given by:

$$\epsilon^* = \epsilon' + i\epsilon''$$

where the complex ϵ'' and the real ϵ' parts are related by the Kramers-Kronig relation.

2.1.4 Dielectric Relaxation

The dielectric relaxation theory for small electric field strengths is a specific application of linear response theory, applicable to isotropic systems. In this context, the time-dependent response $y(t)$ of a system, following a disturbance $x(t)$, is described by a linear equation. For dielectrics, the disturbance is the time-dependent external electric field $x(t) = E(t)$, and the response is the polarization $y(t) = P(t)$. This relationship is given by:

$$P(t) = P_\infty + \epsilon_0 \int_{-\infty}^{t} \epsilon(t-t') \frac{dE(t')}{dt'}\, dt'$$

where $\epsilon(t)$ is the time-dependent dielectric function, and P_∞ includes all contributions from induced polarization. This equation relies on the principles of linearity (the system's response to multiple disturbances is the sum of individual responses) and causality (only past disturbances influence the response at time t).

When a stationary periodic electric field $E(t) = E_0 e^{-i\omega t}$ is applied, the equation transforms to:

$$P(t,\omega) = \epsilon_0 (\epsilon^*(\omega) - 1) E(t,\omega)$$

with the complex dielectric function defined as:

$$\epsilon^*(\omega) = \epsilon'(\omega) - i\epsilon''(\omega)$$

Here, $\epsilon'(\omega)$ represents the energy stored in the system per period, and $\epsilon''(\omega)$ corresponds to the energy dissipated per period. The relationship between the time-dependent dielectric function $\epsilon(t)$ and the complex dielectric function $\epsilon^*(\omega)$ is given by:

$$\epsilon^*(\omega) = \epsilon_\infty - \int_0^\infty \frac{d\epsilon(t)}{dt} e^{-i\omega t}\, dt$$

This expression is a one-sided Fourier or full imaginary Laplace transformation.

2.2 Relaxation in Polymers and Glass Transition

Relaxation processes in polymers are fundamental to understanding their mechanical and electrical behaviors – especially in response to external stimuli such as stress or electric fields. These processes describe the return of polymer chains or segments to equilibrium after being disturbed. The relaxation behavior of polymers is highly dependent on temperature and frequency, leading to distinct relaxation modes.

The two main relaxation processes, based on the time scales and the types of molecular motions involved, are α and β-relaxations.

2.2.1 α-Relaxation

The α-relaxation is linked to large-scale, cooperative motions of polymer chains and is directly associated with the glass transition temperature (T_g) (GTT) in bulk polymers. This relaxation process occurs near or above T_g, where the polymer transitions from a rigid, glassy state to a more flexible, rubbery state.

2.2.2 β-Relaxation

The β-Relaxation is a secondary relaxation process that occurs at temperatures below T_g. It involves localized motions of smaller segments or side groups of the polymer chains, rather than the entire chain. Beta relaxations are typically observed at lower temperatures and are responsible for smaller, more subtle changes in the material's properties compared to alpha relaxation.

2.3 Thin Films

2.3.1 Introduction to Thin Films and the Debate about T_g

Thin films, (i.e. layers of material from nanometers to micrometers thick), are important for the most disparate applications, and thus the subject of many scientific studies. A prominent topic of discussion in the study of thin films is the glass transition temperature T_g. There is an ongoing debate about whether T_g is altered in thin films compared to bulk materials. This debate arises from numerous studies using techniques such as ellipsometry, neutron and X-ray reflectivity, positron annihilation lifetime spectroscopy (PALS), and thermal probe measurements. These studies have reported both increases and decreases in T_g, which hints that the interaction between the polymer and its boundaries can significantly affect its thermal properties. For instance, freely standing films of high molecular weight polystyrene have been studied, with some theories proposing that additional relaxation modes, such as a "sliding motion" of polymer chains near free surfaces, may be responsible for these observed variations. This topic remains under active investigation, with theoretical models and computer simulations continuing to explore the underlying mechanisms affecting the glass transition in thin films, and we will try to contribute to the debate with the data present in this work.

2.3.2 Dynamics in Thin Films

The dynamics of polymers in thin films can differ significantly from those in the bulk due to a variety of factors, including chain stiffness, film thickness, and interactions at the interface. In thin films, especially those with thicknesses on the order of a few nanometers, the confinement effects and proximity to interfaces can lead to much altered molecular dynamics.

Chain stiffness plays a major role in this: while the dynamics in bulk is largely governed by the intrinsic flexibility or stiffness of the polymer chains, thin films, have a reduced dimensionality that can lead to restricted chain mobility, particularly for stiffer polymers (like the ones we are studying in this work). The constraints imposed by the film's boundaries can limit the degree of conformational changes that the polymer chains can undergo, thereby modifying the relaxation processes and overall dynamics.

Another important effect that's accentuated in thin films are interface interactions, because the surface-to-volume ratio is higher, making the influence of the substrate or surrounding medium significant. For polymers with long chain segments, the interface can induce orientation or ordering effects, which are not typically present in the bulk material.

This can lead to the emergence of new relaxation modes or the suppression of bulk relaxation processes. For instance, the sliding motion of polymer chains along their contour, proposed for freely standing films of polystyrene, is an example of how thin film dynamics can introduce mechanisms not observed in bulk polymers.

2.3.3 Deconvolution and Gradient of Relaxation Time in Thin Films

Relaxation time in thin films exhibits a spatial gradient, related to how molecular relaxation processes penetrate into the material from the interface.

A way to analyze this behaviour is using deconvolution techniques, which allow for the separation of overlapping relaxation processes, providing detailed insights into the distribution of relaxation times across different regions of a polymer film. This method is particularly useful when studying thin films, where the relaxation time gradient can vary significantly from the interface into the bulk-like interior of the material.

The relaxation time typically shows a pronounced gradient – starting with values that are either much shorter or much longer than those in the bulk. It then gradually transitions towards bulk-like behavior as one moves away from the interface. Several factors influence this, like chain stiffness and the strength of interactions between the polymer chains and the interface.

Near the interface, the altered mobility of polymer chains, especially in systems with long chain segments, leads to a distinctive dynamic profile. This profile can be captured by advanced models, such as those proposed in recent studies, including the work by Cheng and colleagues **?**. Their study highlights how broadband dielectric spectroscopy (BDS) can be used to reveal the spatial gradient of relaxation times. The data obtained from these analyses provide crucial input for theoretical models, such as the Random First-Order Transition (RFOT) theory and the Elastically Collective Nonlinear Langevin Equation (ECNLE) theory, both of which try to explain the interface-induced modifications in polymer dynamics.

Employing such models is beyond the scope of the present work, but the resulting data can still provide valuable insights and inform future modeling efforts.

2.4 Modeling Functions

When we aim to analyze dielectric spectra, it all comes down to give physical models that give insight into the occurring phenomena. A simple, commonly-used approximation is the model of relaxation time. The most general way to understand it is that the time derivative of a quantity is proportional to the quantity itself. As an instance:

$$\frac{dP(t)}{dt} = -\frac{P(t)}{\tau_D}$$

where τ_D is the characteristic relaxation time. Solving this equation yields an exponential decay for the correlation function $\Phi(\tau)$:

$$\Phi(\tau) = \exp\left(-\frac{\tau}{\tau_D}\right)$$

This leads to the following complex dielectric function $\epsilon^*(\omega)$:

$$\epsilon^*(\omega) = \epsilon_\infty + \frac{\Delta\epsilon}{1 + i\omega\tau_D} \tag{2.5}$$

where $\Delta\epsilon = \epsilon_S - \epsilon_\infty$ is the dielectric relaxation intensity, with $\epsilon_S = \lim_{\omega\to 0} \epsilon'(\omega)$ and $\epsilon_\infty = \lim_{\omega\to\infty} \epsilon'(\omega)$.

The Debye relaxation time τ_D is related to the position of maximal loss by

$$\omega_p = \frac{2\pi}{\nu_p} = \frac{1}{\tau_D} \tag{2.6}$$

Equation 2.5 is known as Debye relaxation, and is the basis for further models we will discuss next.

2.4.1 Expanding on the Debye Model

The Debye model above is, however, not sufficient to describe all the effects that happen within the dielectric spectra in most cases. Therefore, non-Debye models have been introduced, and a short outline will be discussed below.

A commonly used model is the Cole-Cole function, given by:

$$\epsilon^*_{\mathrm{CC}}(\omega) = \epsilon_\infty + \frac{\Delta\epsilon}{1 + (i\omega\tau_{\mathrm{CC}})^\beta}$$

where $0 < \beta \leq 1$. This function introduces a symmetrical broadening of the relaxation function, with the Debye function recovered when $\beta = 1$. The characteristic relaxation time τ_{CC} determines the position of maximal loss, defined analogously as in Equation 2.6.

For cases where the dielectric function exhibits asymmetric broadening, the Fuoss-Kirkwood or Cole-Davidson functions are more appropriate. The Cole-Davidson function is expressed as:

$$\epsilon^*_{\mathrm{CD}}(\omega) = \epsilon_\infty + \frac{\Delta\epsilon}{(1 + i\omega\tau_{\mathrm{CD}})^\gamma}$$

Here, $0 < \gamma \leq 1$ introduces asymmetry, with the Debye function being a special case when $\gamma = 1$. The characteristic relaxation time τ_{CD} does not necessarily correspond to the position of maximal loss, which is instead given by:

$$\omega_p = \frac{1}{\tau_{\mathrm{CD}}} \tan\left(\frac{\pi}{2\gamma + 2}\right)$$

2.4.2 The Havriliak-Negami Function

A more general approach is provided by the Havriliak-Negami (HN) function, which combines features of both the Cole-Cole and Cole-Davidson functions:

$$\epsilon^*_{\mathrm{HN}}(\omega) = \epsilon_\infty + \frac{\Delta\epsilon}{(1 + (i\omega\tau_{\mathrm{HN}})^\beta)^\gamma}$$

In the HN function, $0 < \beta, \gamma \leq 1$, where β and γ describe the symmetric and asymmetric broadening, respectively. The behavior of the dielectric function at low and high frequencies, $\epsilon_S - \epsilon'(\omega) \sim \omega^m$ and $\epsilon'' \sim \omega^m$ for $\omega \ll 1/\tau_{\mathrm{HN}}$, is characterized by the exponent $m = \beta$.

The dielectric function's behavior at high frequencies can be described by the following relationships:

$$\epsilon'(\omega) - \epsilon_\infty \sim \omega^{-n} \quad \text{and} \quad \epsilon'' \sim \omega^{-n} \quad \text{for} \quad \omega \gg \frac{1}{\tau_{\mathrm{HN}}}$$

with $n = \beta\gamma$. The parameters m and n, introduced by Jonscher, represent the slopes of $\log\epsilon''$ versus $\log\omega$ at low and high frequencies, respectively, relative to the position of maximal loss.

The position of maximal loss ω_p depends on the shape parameters β and γ as follows:

$$\omega_p = \frac{1}{\tau_{\mathrm{HN}}}\left[\sin\left(\frac{\beta\pi}{2+2\gamma}\right)\right]^{\frac{1}{\beta}}\left[\sin\left(\frac{\beta\gamma\pi}{2+2\gamma}\right)\right]^{-\frac{1}{\beta}}$$

and therefore,

$$\tau_c(\beta,\gamma) = \tau_{HN}\left[\sin\left(\frac{\pi\beta\gamma}{2+2\gamma}\right)\right]^{-\frac{1}{\beta}}\left[\sin\left(\frac{\pi\beta}{2+2\gamma}\right)\right]^{\frac{1}{\beta}}$$

corresponds to the relaxation time at maximum loss peak.

2.5 The Derivative Method

Due to the significant conductivity contribution, which obscures the clear observation of the loss peak near the glass transition temperature, the derivative method has to be employed. This consists in exploiting the Kramers-Kronig (KK) relation to our advantage: since the integral transform of ϵ' doesn't include the (ionic) Ohmic conduction term, it will contain the same information as ϵ'' without this conductivity contribution.

An easy way to interpret ϵ' is to take its derivative and using the relationship:

$$\epsilon''_{\mathrm{der}} = \left(-\frac{\pi}{2}\right)\frac{d\epsilon'}{d\ln f} \approx \epsilon''_{\mathrm{rel}}$$

which means that the HN function for the derivative of ϵ' will have the form:

$$\frac{\partial\epsilon'_{\mathrm{HN}}}{\partial\ln f} = -\frac{\beta\gamma\Delta\epsilon\cdot(2\pi f\tau)^{\beta}\cos\left[\beta\frac{\pi}{2}-(1+\gamma)\theta_{\mathrm{HN}}\right]}{\left[1+2(2\pi f\tau)^{\beta}\cos\left(\frac{\beta\pi}{2}\right)+(2\pi f\tau)^{2\beta}\right]^{(1+\gamma)/2}}$$

where

$$\theta_{\mathrm{HN}} = \arctan\left[\frac{\sin(\pi\beta/2)}{(2\pi f\tau)^{-\beta}+\cos(\pi\beta/2)}\right]$$

and the rest of the parameters are defined as before.

2.5.1 Our Fitting Function for the BDS Data

Based on these considerations, the fitting function for our data will have the following form:

$$F(\Delta\epsilon_i,\tau_{\mathrm{HN}_i},\beta_i,\gamma_i,\sigma_0,a) = \sum_{i=1}^{3}\left(\frac{\partial\epsilon'_{\mathrm{HN}}}{\partial\ln f}\right)_i + \frac{\sigma_0}{\epsilon_0\omega^a} \tag{2.7}$$

where the first term consists in multiple HN functions which are summed together – up to three, depending on the number of peaks in the spectrum – and the second term indicates the electrode polarization (EP), which usually happens at low frequencies before the first HN peak, and has the form of a DC conductivity, but is not always occurring and thus optional.

2.6 The VFT Function

The Vogel-Fulcher-Tamann (VFT) equation is a widely used empirical formula that describes the temperature dependence of the relaxation time τ in polymers. It is given by:

$$\log_{10} \tau = \log_{10} \tau_\infty - \frac{D_T T_0}{T - T_0}$$

where τ is the relaxation time, T is the temperature, τ_∞ is the relaxation time at infinite temperature, D_T is a material-specific constant (often referred to as the fragility parameter), and T_0 is the Vogel temperature, which is typically below the GTT. We will make use of this equation to describe the relaxation time behavior of our samples, and check for a thickness dependence in the GTT.

Chapter 3

Methods & Materials

3.1 The Polymers in Question

Two different polymers are analyzed in this work: Poly([N,N'-diphenyl-N,N'-bis(4-tert-butylphenyl)-(1,1'-biphenyl)-4,4'-diamine]-alt-formaldehyde) (Poly-TPD) and 4,4-Dihydroxydiphenyl-2,2-propane carbonate polymer (Poly-Bisphenol).

3.1.1 Poly-TPD

Poly-TPD is from the supplier Polymer Source, Inc.™ with the sample number P16210-PolyTPD-FA, has a $M_n = 28.500$, and $M_w = 32.000$. It consists of triarylamine (TPD) with fluorene (FA) units incorporated into its backbone. The chemical structure can be described by the repeating units:

$$(C_{15}H_{11}N) - (C_{13}H_8)_n$$

This polymer contains an FA conjugated backbone that is critical for its semiconducting properties. In particular its high hole mobility, in the range of 10^{-4} to 10^{-3} cm^2/Vs, makes it suitable for use as a hole transport layer (HTL) in organic light-emitting diode (OLED) and organic photovoltaic (OPV) devices.

As for its thermodynamic properties, Poly-TPD exhibits good thermal stability, with a decomposition temperature $T_d > 350$°C, and a glass transition temperature around 90-150°C.

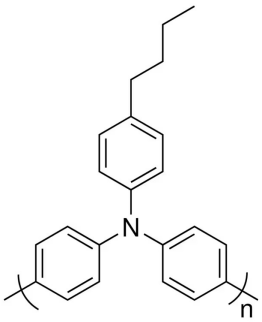

Figure 3.1: Chemical structure of Poly-TPD

3.1.2 Poly-Bisphenol

Poly-Bisphenol, on the other hand, came from the manifacturer Sigma-Aldrich®, with the sample code 181625-250G Poly(Bisphenol A carbonate), and has a $M_w \approx 45.000$ by gel permeation chromatography (GPC). Its glass transition temperature is $T_g \approx 150°C$, and melting point $T_m \approx 267°C$. It has the repeating unit (or monomer)

$$C_{15}H_{16}O_2$$

and is a thermoplastic polymer with optical clarity, high tensile strength/impact resistace, high refractive index, and it is used, for example, to prepare optical lenses or as a supporting matrix to fabricate hybrid nanofiber membranes.

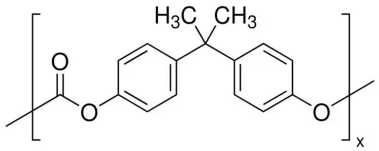

Figure 3.2: Chemical structure of Poly-Bisphenol

3.2 Preparation of the samples

The preparation of the samples required for our analysis involves creating parallel-plate capacitors on a glass substrate. These capacitors have an area of approximately 6×6 mm and a thickness that varies from around 300 nm to 5 nm.

Controlling the thickness of the dielectric material within the capacitor is particularly important, as our goal is to study the effects of thin layers compared to the bulk material. This control is achieved by preparing polymer solutions with different concentrations: the higher the concentration, the thicker the resulting film.

3.2.1 Solution Preparation

In particular, 7 solutions were prepeared for each of the polymers starting from a concentration of 20mg/ml and roughly halvened. The solvent used for Poly-TPD was Chloroform ($CHCl_3$, manifacturer Sigma-Aldrich®, sample number C2432-1L), while Poly-Bisphenol was diluted in Dichloromethane (CH_2Cl_2, manifacturer Sigma-Aldrich®, sample number 32222).

As an example, to compute the volume required to dilute a solution from an initial concentration of 20 mg/ml to a desired concentration of 10 mg/ml, with a final volume of 10 ml, we use the dilution formula:

$$C_1V_1 = C_2V_2$$

where:

$$C_1 = 20\,\text{mg/ml} \quad \text{(initial concentration)}$$

$$C_2 = 10\,\text{mg/ml} \quad \text{(desired concentration)}$$

$$V_1 = \text{unknown volume (to be calculated)}$$

$$V_2 = 10\,\text{ml} \quad \text{(final volume)}$$

Table 3.1: Concentrations and volumes of both sets of solutions (Poly-TPD and P-Bisphenol)

C (mg/ml)	$V_{solution}$ (ml)	$V_{solvent}$ (ml)
10	5	5
3	3	7
1	3	6
0.5	4	4
0.2	4	6
1	5	5

Substituting the known values:

$$20\,\text{mg/ml} \times V_1 = 10\,\text{mg/ml} \times 10\,\text{ml}$$

Solving for V_1:

$$V_1 = \frac{10\,\text{mg/ml} \times 10\,\text{ml}}{20\,\text{mg/ml}} = \frac{100\text{ml}}{20} = 5\,\text{ml}$$

This was done similarly for all other solutions, and the resulting concentrations are shown in Table 3.1

3.2.2 Preparation of the Substrate

The glass substrates were prepared by cutting standard microscope slides into approximately 1×1 cm squares, followed by cleaning in an ultrasonic cleaner using ethanol and deionized water. This cleaning process ensures a contaminant-free surface for the deposition of polymer solutions. After cleaning, the substrates were dried using pressurized N_2 in a laminar flow hood to avoid dust contamination and then stored in a Petri dish.

Once the substrates were prepared, the next step was to create the first of the two plates of the capacitors. This was accomplished by depositing gaseous aluminum in approximately 5 mm wide strips across the substrate. Specifically, to produce a total of 9 capacitors, three equally spaced strips of aluminum were deposited. This was done using a complementary mask, which covered all areas of the substrate except for where the strips were intended to be, ensuring that the evaporated aluminum only adhered to the exposed glass surface.

The thermal evaporation process used for this deposition is relatively straightforward. It involves melting a small quantity of aluminum (in our case, taken from tiny cut wire) in a turbomolecular-pump vacuum chamber by heating a tungsten base with a high current. This results in the desired evaporation of the metal and its subsequent surface accumulation. The thickness of this accumulation can be controlled by adjusting the duration of the current applied to the tungsten base. In our case, just a few seconds of heating produced an aluminum layer approximately 200 nm thick.

3.2.3 Spin-Coating of the Solution

Once the first of the two aluminum capacitor plates is deposited on the glass substrate, the next step is to apply the dielectric material between the plates. This is achieved by depositing the respective

polymer solution onto the plate. The spin-coating technique is particularly useful in this case, as it ensures a uniform distribution of the solution across the glass layer.

In our procedure, a spin-coating program of 1 minute at 4000 rpm was used for all polymer solutions to ensure reproducibility.

Moreover, the glass slides were marked appropriately to allow for distinction of polymer and concentration at a later time.

3.2.4 Heating and Annealing

After spin-coating the solution, the samples were placed in a small glass container, which was then evacuated to remove any trapped air or moisture. The container was subsequently placed inside an oven set to 200°C and maintained at this temperature for 12 hours to allow for annealing.

Annealing is useful for improving the film's uniformity and adhesion to the substrate, enhancing its mechanical properties, and promoting the removal of residual solvents. It also helps in stabilizing the polymer film by allowing the polymer chains to rearrange and settle into a more stable configuration.

After this process, aluminum was evaporated a second time in strips perpendicular to the earlier ones, completing the fabrication of the capacitors.

Figure 3.3: Deposition of the aluminum on the glass substrate

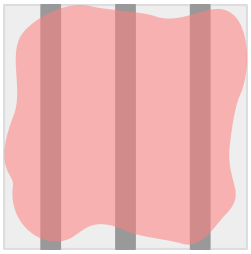

Figure 3.4: Spin-coating of the polymer solution

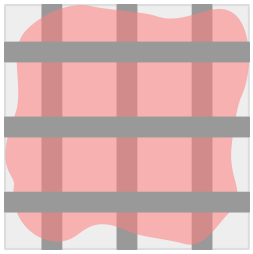

Figure 3.5: Second deposition of aluminum, perpendicularly on top

3.3 Atomic Force Microscopy

The use of Atomic Force Microscopy (AFM) is particularly useful when measuring the thickness of the dielectric in our samples. This measurement is essential due to the capacitance formula for a parallel-plate capacitor:

$$C = \epsilon \frac{A}{d}$$

where ϵ is the permittivity, A is the surface area of the plate, and d is its thickness. Since dielectric measurements rely on this formula, both A and d must be accurately determined. The former is a straightforward parameter to obtain, and in our case, it was measured using a simple optical microscope.

The measurement of the latter, however, is more challenging and cannot be obtained by the initial concentration of the spin-coated solution, as this would be overly imprecise and unreliable.

To accurately determine the thickness, AFM is employed in the following manner:

1. The surface of the sample is first scratched with a needle in a non-capacitor region (i.e., where no aluminum is present) as shown in the figure. This scratch allows for the measurement of the thickness of the deposited polymer layer.

2. The scratched area is then positioned under the AFM tip, with approximately half of the scratched region occupying the field of view and the non-scratched region occupying the other half.

3. This setup allows for the measurement of the relative height between the substrate and the polymer film, which is then analyzed using Gwyddion, where a simple statistical average of the two heights can be calculated, providing a relatively accurate thickness of the dielectric.

This process was repeated two or more times for each sample, and the resulting thicknesses were then averaged for each of the capacitors. The results of these measurements are presented below.

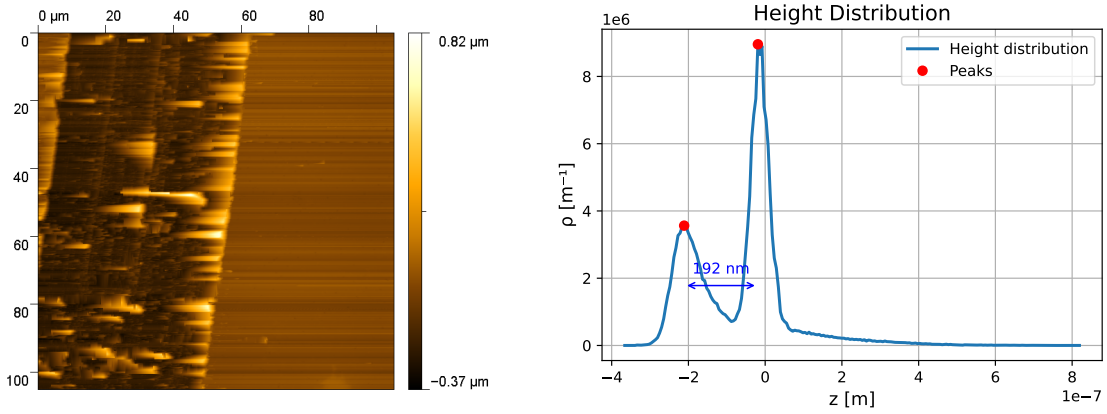

(a) AFM picture of the scratched film

(b) height distribution

Figure 3.6: Poly-TPD thin film, sample A (200nm), example of a height distribution and AFM picture.

3.4 Dielectric Spectroscopy

Once we know the parameters of our samples, we can move to the actual BDS measurements. This technique enables to obtain (among other things) the frequency and temperature-dependent complex and real parts of the DF ϵ^*, from which molecular dipole dynamics, polarization phenomena, and relaxation processes can be deduced. In our case, the frequency range was set up to be from 10^{-1}Hz to 10^6Hz, and a temperature from about 290K to 530K.

A frequency generator takes care of the AC current input, with a root mean square (RMS) voltage $V_{RMS} = 0.1$V, while temperature is controlled using a Dewar flask containing liquid nitrogen, and resistances that are heated depending on the wanted temperature. The temperature of the sample is then measured using a platinum resistance thermometer, which allows for a very precise sensing of T (with an error of less than 1K).

Proper attention must be given to the connection between the sample and the BDS setup. This is achieved by using copper/gold terminals that are secured to the aluminum surface of the capacitor plates with screws, ensuring firm contact with the glass slide. Careful attention is given to ensure that the resistance is less than 2Ω across the plate and the BDS terminals, and $>$ 20MΩ between the two plates (otherwise it would be counted as a shorted capacitor).

That done, the sample holder is placed in the setup and the measurement can be started, lasting about 18 hours for the whole temperature range to be recorded on both heating and cooling, such that reproducibility is guaranteed. However, especially in thinner films, it was noted that the sample undergoes some dielectric changes after being exposed to rapid and repeated temperature fluctuations.

Chapter 4

Results & Discussion

4.1 Obtained Dielectric Spectra

The final dielectric spectra are plotted in Figures 4.1, B.1, B.2 and B.3 for the various thicknesses of Poly-TPD and B.4, B.5 and **??** for Poly-Bisphenol, along with the derivative of epsilon prime.

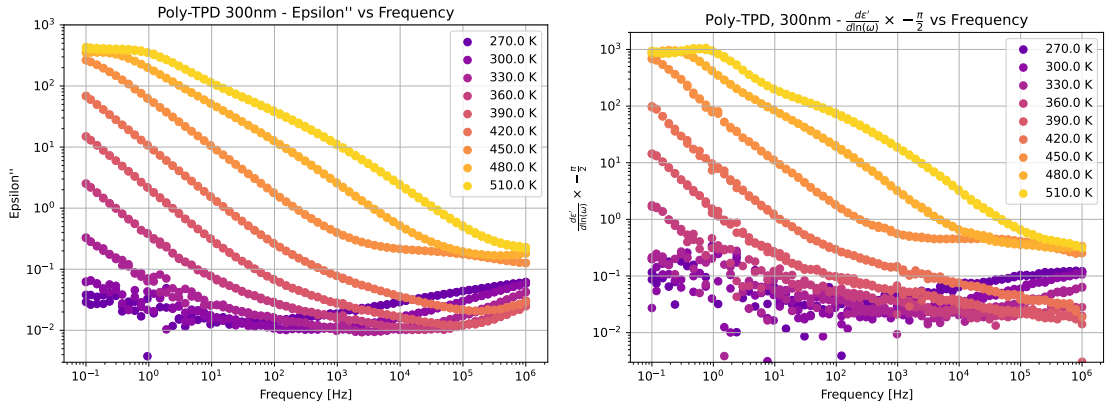

(a) ϵ'' vs. f

(b) derivative of ϵ' vs. f

Figure 4.1: 200nm Poly-TPD thin film, complex dielectric function and derivative of the real part as a function of frequency at different temperatures (plotted once every 30 kelvin for clarity).

4.1.1 Qualitative Observations

A quick overview at the obtained spectra brings one to notice the following traits:

- The derivative plot is generally more helpful in identifying the occurring peaks, which are more pronounced with respect to the ϵ'' plot. This happens because of the removal of Ohmic conductivity, as discussed earlier.
- At low temperature, the plots become more imprecise, probably due to a combination of the electronic oscillations and computation artifacts in the case of the derivative. In some cases, a spline interpolation was used to make the data more suitable for the subsequent fitting.

- Thinner films generally exhibit a breakdown (i.e. shorting) at lower temperatures, although not always (as was the case of the 320nm Poly-Bisphenol film). This is consistent with the expectation that higher temperatures facilitate the penetration of the aluminum layers in the polymer, which becomes more conductive and eventually leads to a short circuit. Also the thermal expansion of aluminum might be playing a role, though it should only be relevant for the thinner films, as its range of action is $\approx$ 5nm.

4.2 Fitting of the Data

The derivative of ϵ' was then fit using Python according to Equation 2.7, for each temperature value every 10K, in a range where the data was reasonably clean (i.e. did not contain too much noise). One example of such fitted plot is shown below for the 200nm Poly-TPD (the other ones can be found in the Appendix).

4.3 Discussion about the Obtained Parameters

4.3.1 Relaxation Times

The relaxation time τ is a parameter of interest that we draw from the HN function fitting. We will now discuss the retrieved τ's for the different polymers.

Poly-TPD

Three relaxation processes are visible in the spectra of this polymer, which were thus fit with three independent HN functions, named HN1,2,3 from lowest frequency to highest. It was interesting to note that these relaxation times do not always depend on thickness. This was the case for τ_{HN1}, in Figure 4.2, for which there is a coincidence (up to some noise) of the relaxation times for different thicknesses.

A different situation occurs for τ_{HN2}, which instead shows a clear thickness dependence: for low thicknesses, τ_{HN2} is much smaller than the higher counterparts. Moreover, it is reasonable to believe that a saturation may occur for very thick films (bulk), as the difference between the τ's becomes much smaller when going from the 110nm to 200nm film, than from 8nm to 24nm, as seen in Figure 4.3.

The high frequency relaxation times modeled by the HN3 function are plotted in Figure 4.4, and also show a thickness dependence, but there's an overlap between the 24nm and 110nm that is not immediately explainable if not by fitting errors. Indeed, since this third peak is generally broader for all spectra, there is greater chance of the parameters being not as clearly definable as for the previous, less wide peaks.

Poly-Bisphenol

The low-frequency relaxation times are plotted in Figure 4.5, and look like being thickness-independent, as with Poly-TPD. In this case, the 43nm measurement was deemed inaccurate because, as seen in e.g. Figure **??**, the first peak occurs outside of the spectrum, and it's difficult to pinpoint the exact τ from just fitting. For the 14nm and 320nm, where this doesn't occur (at least at higher temperatures), the correspondence is much more apparent.

The second process (Figure 4.6) is utterly thickness dependent, and we note a behaviour similar as for Poly-TPD: lower relaxation time for lower thickness, and vice versa. The 2nd peak for the 14nm

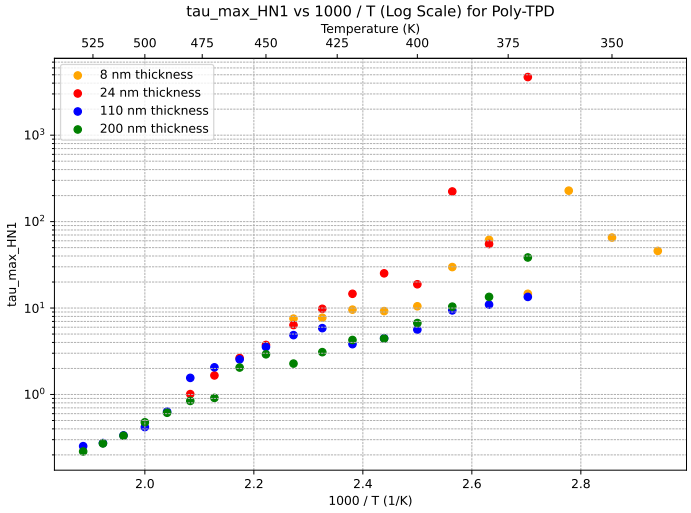

Figure 4.2: Relaxation times of the first relaxation process (i.e. obtained from the HN1 function) occurring in Poly-TPD at different thicknesses. This process seems to not depend on thickness and the different values of tau were ascribed to fitting error/noise.

film, as seen in **??**, was very much hidden by the other peaks, and not strongly visible, which is why it changes so abruptly with respect to the other ones. Still, the main difference between bulk and thin film is well-defined.

Similarly as before, the high frequency (HN3) process has a somewhat thickness-dependent relaxation time, but the relationship is again nontrivial, as seen in Figure 4.7. Further experimentation is deemed necessary to better understand this behaviour.

VFT fit of the relaxation times

To interpret the relaxation times, we make use of the VFT equation, as defined earlier. The fitting of the τ_{HN2} functions at different thicknesses is shown in Figure 4.8 for Poly-TPD and Figure 4.9 for Poly-Bisphenol, and the parameters are represented in Tables 4.1 and 4.2, respectively. Genrally speaking, an increase (in absolute value) with thickness seems to correlate all of the obtained parameters.

Of particular interest is then computing the GTT, which we define as the temperature at which τ is equal to 10s. There is actually a debate on whether this definition is reliable or not, and some studies often define the GTT as T for $\tau = 100$s. Nonetheless, in this work, the former definition was chosen, as the resulting T_g values resembled more closely the actual values from differential scanning calorimetry (DSC) experiments. Indeed,

4.3.2 α and β-Relaxation and Dielectric strengths $\Delta\epsilon$

Another useful plot for the determination of the temperature at which relaxation processes occur is fixing one frequency and plotting ϵ'' versus T. This was done for the bulk films of both polymers at a frequency of about 1kHz and is shown in Figure 4.10a (Poly-TPD) and Figure 4.10b (Poly-Bisphenol). As noticeable, there are no main peaks in the measured temperature range, which suggests that a greater range might be needed to show the relaxation processes. Yet, in the case of Poly-Bisphenol, a peak appears at the very edge of the spectrum, around T=450K, which corresponds to the α-relaxation

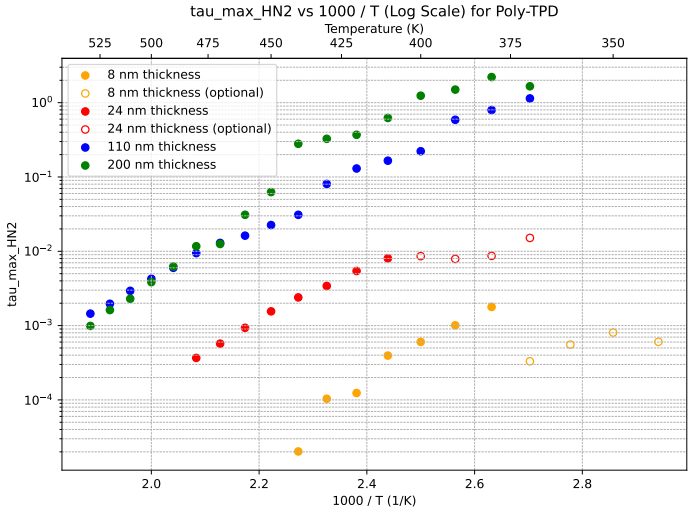

Figure 4.3: Relaxation times of the second relaxation process (i.e. obtained from the HN2 function) occurring in Poly-TPD at different thicknesses. This relaxation process suggests a thickness dependence which is discussed in the following.

Table 4.1: Fitting Parameters for Poly-TPD at Various Thicknesses

Thickness (nm)	log10(τ_∞)	DT	T0 (K)	T_g (T at $\tau = 10$s (K))
8	-15.8875	-147223.1348	0.0342	298.47
24	-11.2485	-248118.7770	0.0152	308.11
110	-9.6441	-292768.5995	0.0124	340.89
200	-11.2431	-659454.5989	0.0068	364.63

process. This same temperature value is also confirmed in the study, and can be used as a double check for the accuracy of the gathered data.

No literature is known at the time of writing for the case of Poly-TPD, but it was considered appropriate to also show the plot, which, if anything, demonstrates that the α-relaxation occurs above 530K, and the β-relaxation below 250K.

4.4 Revisiting the Glass Transition Temperature Debate

The results from our data analysis provide an insight into the ongoing debate regarding the GTT in thin films compared to bulk materials. Specifically, our findings indicate a noticeable difference between the T_g of thin and thick films in both Poly-TPD and Poly-Bisphenol. This disparity can be attributed to the inherent stiffness of the polymer chains, which for these two polymers is particularly prominent.

Indeed, given the stiff nature of these polymers, the T_g observed in the bulk is not directly translatable to the T_g in thin films. The confined geometry of the thin films induces additional relaxation processes that are not present in the bulk material. These processes likely arise from the altered mo-

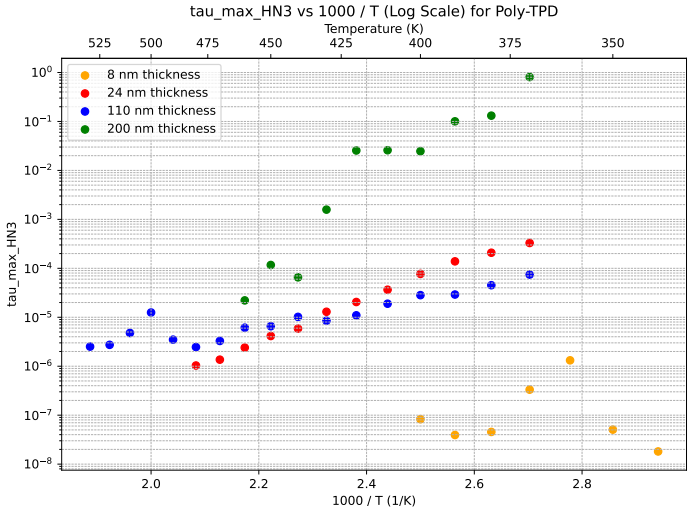

Figure 4.4: Relaxation times of the third relaxation process (i.e. obtained from the HN3 function) occurring in Poly-TPD at different thicknesses. This relaxation process also looks to have a thickness dependence, although not as clear as the second relaxation process.

Table 4.2: Fitting Parameters for Poly-Bisphenol at Various Thicknesses. The 14nm sample is likely unreliable, as discussed in the present section, and was marked in red.

Thickness (nm)	log10(τ_∞)	DT	T0 (K)	T_g (T at $\tau = 10$s (K))
320	-5.2618	-2.4972	253.1543	354.11
43	-7.0539	-6.2055	160.1424	283.53
14	-6.0000	-0.9118	317.1379	358.45

bility and constrained dynamics of the polymer chains near the interfaces, leading to a deviation in the T_g compared to bulk samples.

This observed difference underscores the importance of accounting for these additional relaxation mechanisms when analyzing and predicting the behavior of thin polymer films. The presence of such relaxation processes in thin films suggests that they are governed by dynamics distinct from those of the bulk, necessitating a more nuanced approach to understanding the glass transition and associated thermal properties in nanoconfined systems.

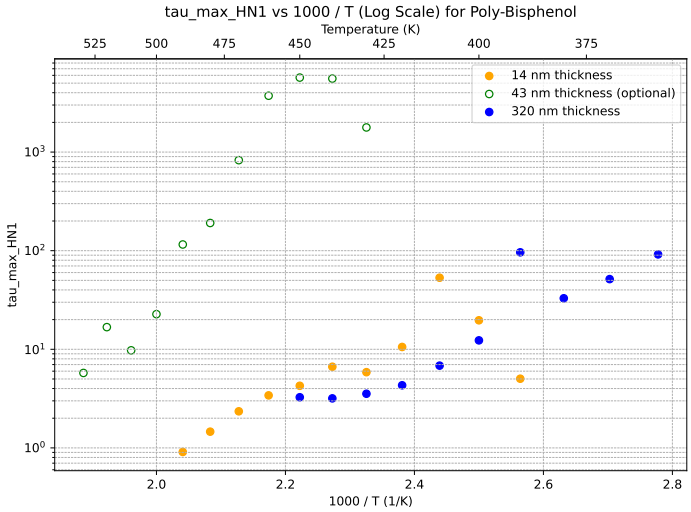

Figure 4.5: Relaxation times of the first relaxation process (i.e. obtained from the HN1 function) occurring in Poly-Bisphenol at different thicknesses. This process appears to depend on thickness in a not-immediately-clear way. Further research may be needed for understanding this fully.

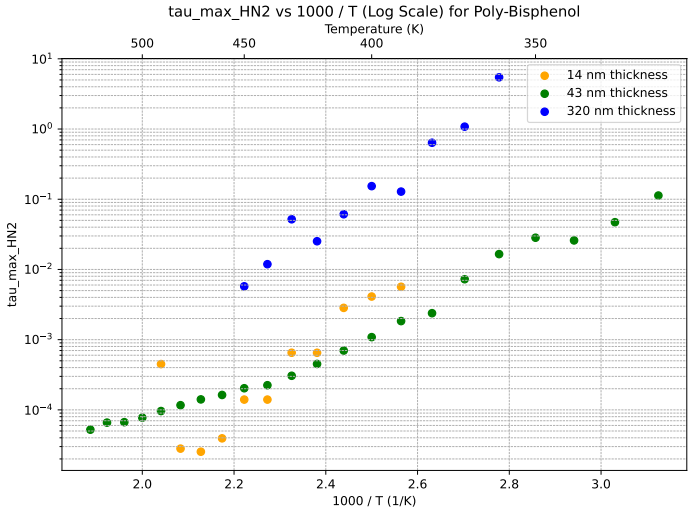

Figure 4.6: Relaxation times of the second relaxation process (i.e. obtained from the HN2 function) occurring in Poly-Bisphenol at different thicknesses. This relaxation process has a clear thickness dependence and is discussed in the following.

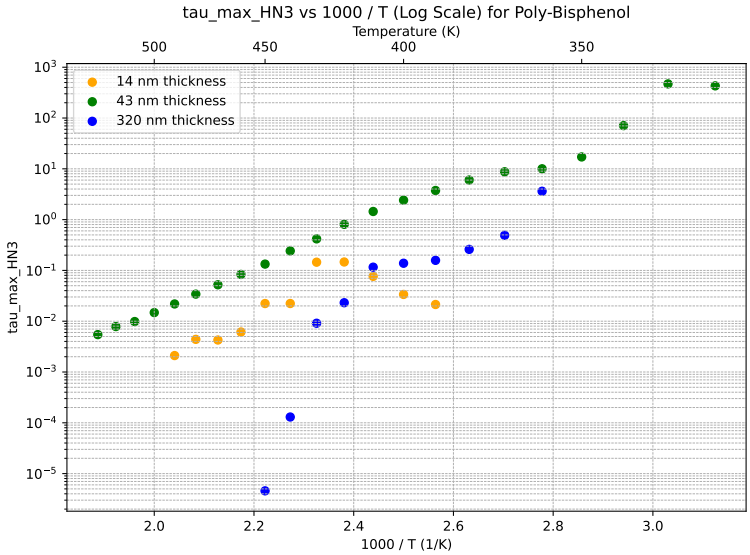

Figure 4.7: Relaxation times of the third relaxation process (i.e. obtained from the HN3 function) occurring in Poly-Bisphenol at different thicknesses. It is still not clear whether the thickness correlation has a physical meaning or is simply due to e.g. errors in the fit.

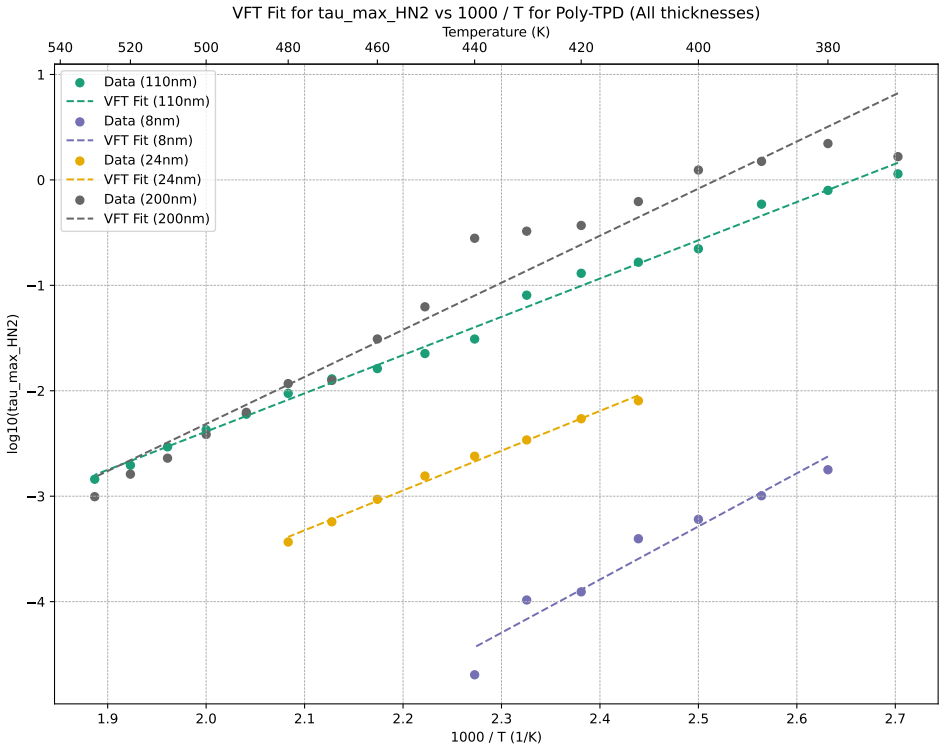

Figure 4.8

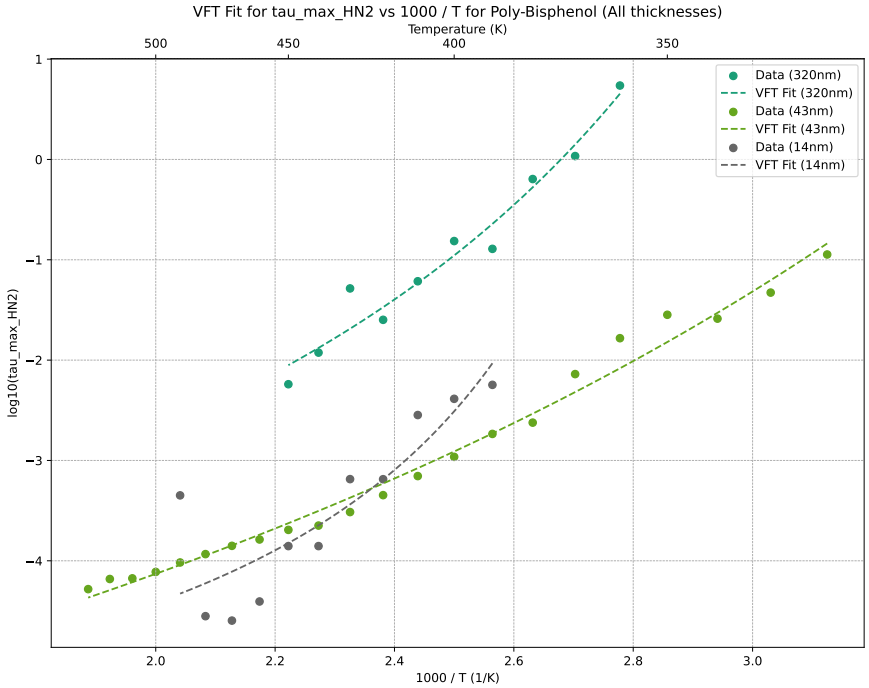

Figure 4.9

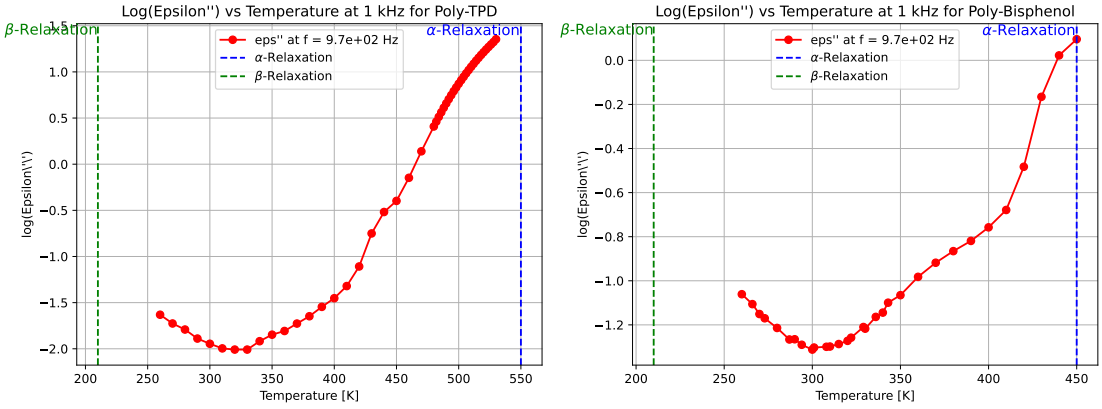

(a) Poly-TPD, 200nm film

(b) Poly-Bisphenol, 320nm film

Figure 4.10: Comparison of ϵ'' vs. T for bulk Poly-TPD and Poly-Bisphenol films at $f \approx 1$kHz.

Chapter 5

Synopse

Dissertation for the attainment of the academic degree:
Bachelor of Science

Dynamics of phenyl-based polymer chains confined in thin layers

submitted by:
Federico Porcelli

prepared in:
IPSP Leipzig

supervised by:
Dr. Martin Treß

September 2024

Declaration of Independent Work

I hereby declare that I have completed the present work independently and without any unauthorized assistance or use of sources other than those specified. I affirm that no third party has received any monetary compensation from me, either directly or indirectly, for work related to the content of this dissertation, and that the submitted work has not been presented in the same or a similar form to any other examination authority, either domestically or abroad, for the purpose of obtaining a degree or other certification. All material taken from other sources or from other individuals that has been used in this work or directly referenced has been clearly marked as such. In particular, all individuals who directly contributed to the creation of this work have been acknowledged.

Leipzig, September 11, 2024

Federico Porcelli

Appendix A

AFM Data

Appendix B

BDS Data

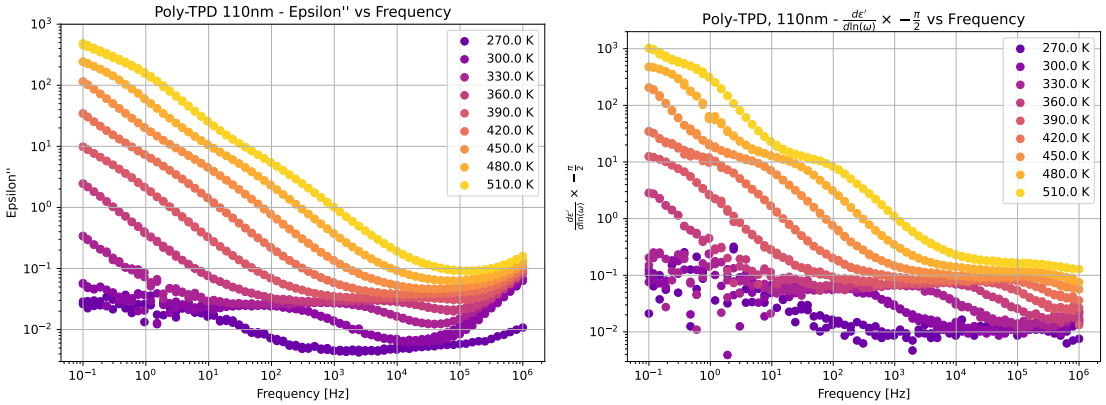

(a) ϵ'' vs. f

(b) $-\frac{\pi}{2}\frac{d\epsilon'}{d(\ln(\omega))}$ vs. f

Figure B.1: 110nm Poly-TPD thin film

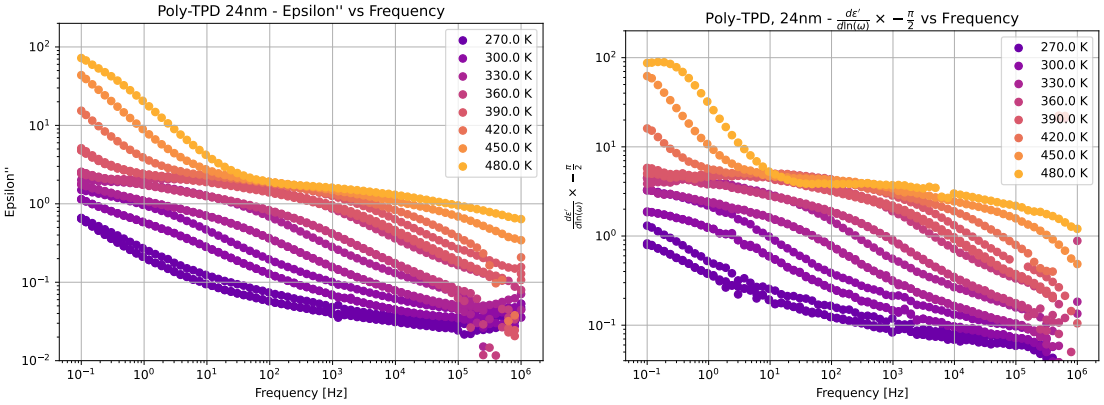

(a) ϵ'' vs. f

(b) $-\frac{\pi}{2}\frac{d\epsilon'}{d(\ln(\omega))}$ vs. f

Figure B.2: 24nm Poly-TPD thin film

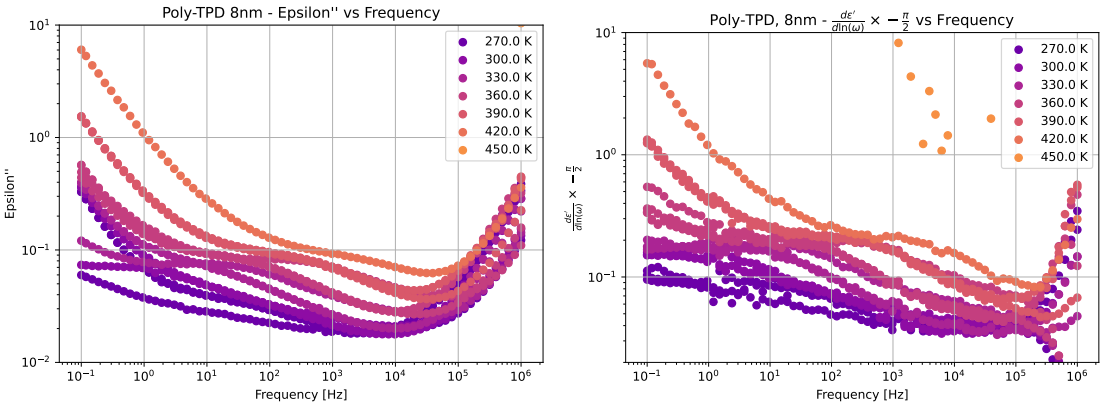

(a) ϵ'' vs. f

(b) $-\frac{\pi}{2}\frac{d\epsilon'}{d(\ln(\omega))}$ vs. f

Figure B.3: 8nm Poly-TPD thin film

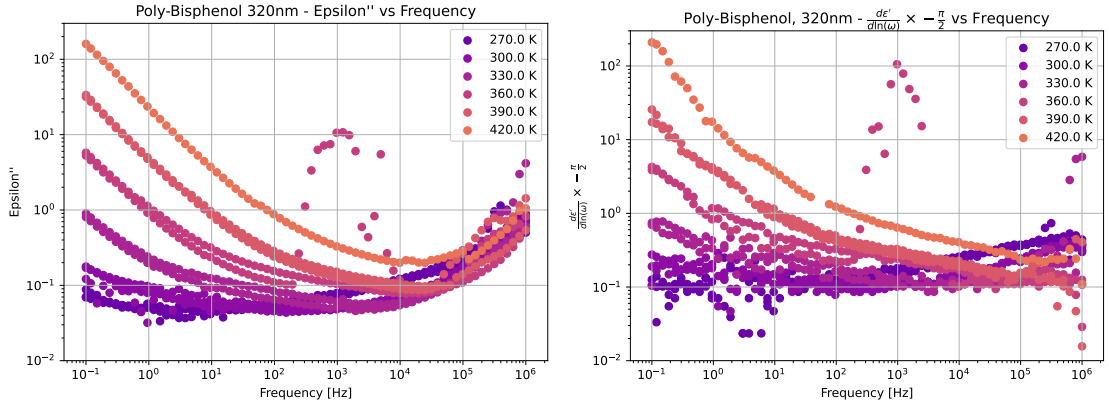

(a) ϵ'' vs. f

(b) $-\frac{\pi}{2}\frac{d\epsilon'}{d(\ln(\omega))}$ vs. f

Figure B.4: 320nm Poly-Bisphenol thin film

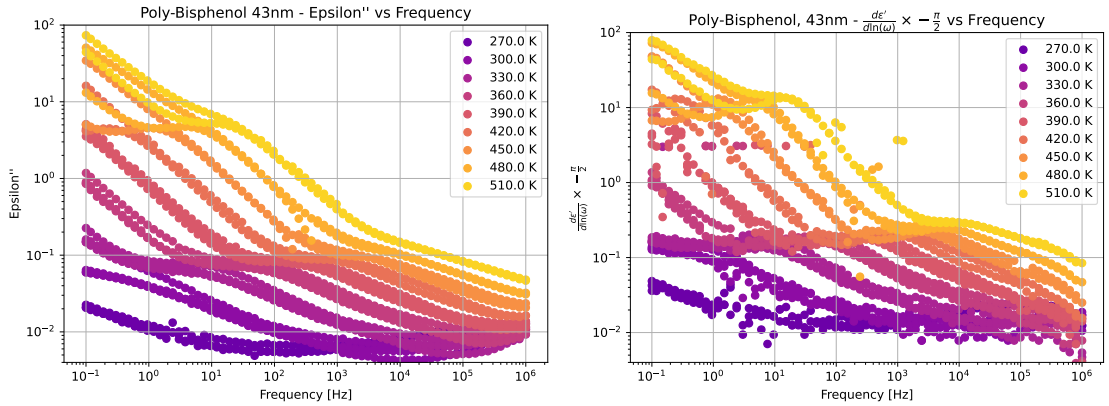

(a) ϵ'' vs. f

(b) $-\frac{\pi}{2}\frac{d\epsilon'}{d(\ln(\omega))}$ vs. f

Figure B.5: 43nm Poly-Bisphenol thin film

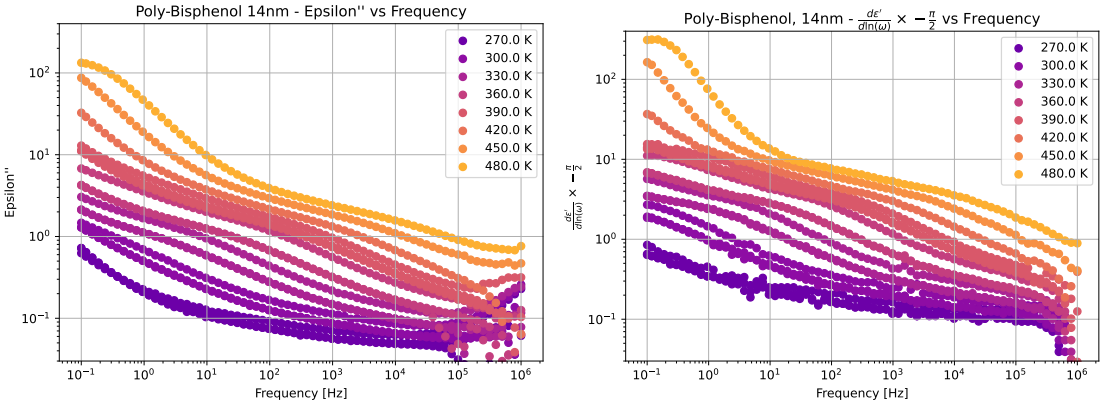

(a) ϵ'' vs. f

(b) $-\frac{\pi}{2}\frac{d\epsilon'}{d(\ln(\omega))}$ vs. f

Figure B.6: 14nm Poly-Bisphenol thin film

Appendix C

Fits of the BDS Data

C.1 Poly-TPD, 200nm thin film

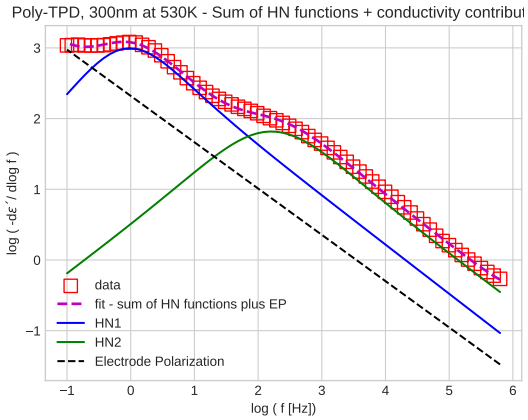

(a) 530K

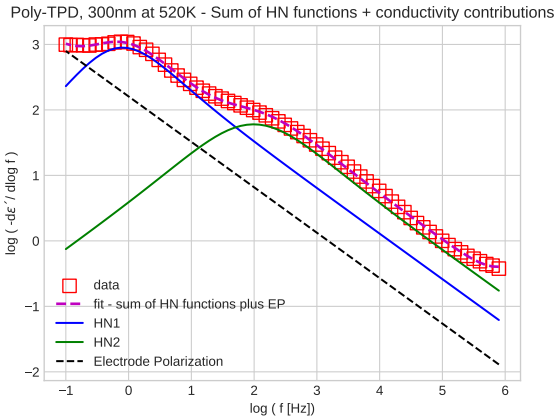

(b) 520K

C.2 Poly-TPD, 200nm thin film

C.3 Poly-Bisphenol, 43nm thin film

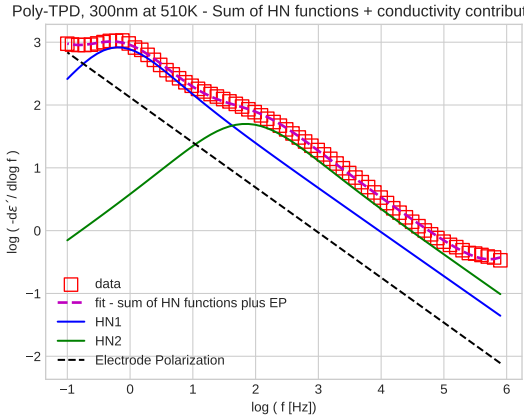

(a) 510K

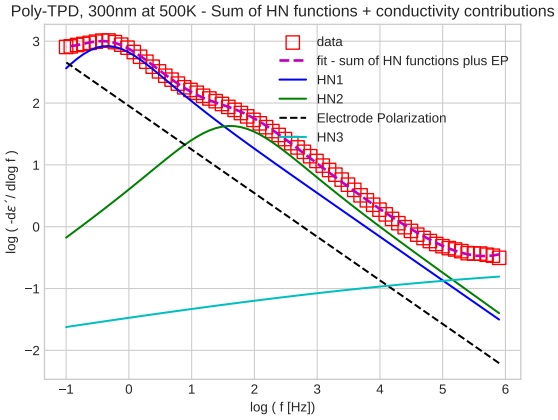

(b) 500K

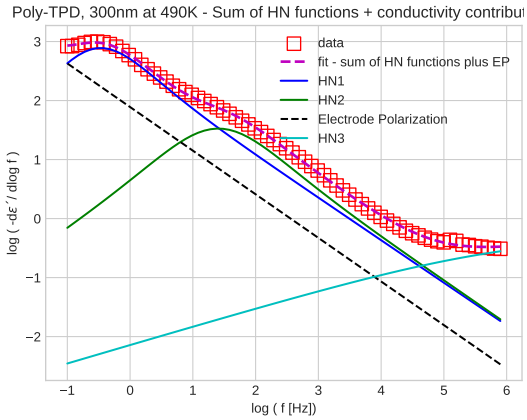

(a) 490K

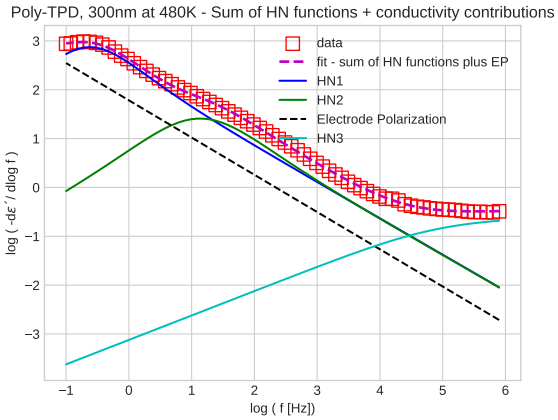

(b) 480K

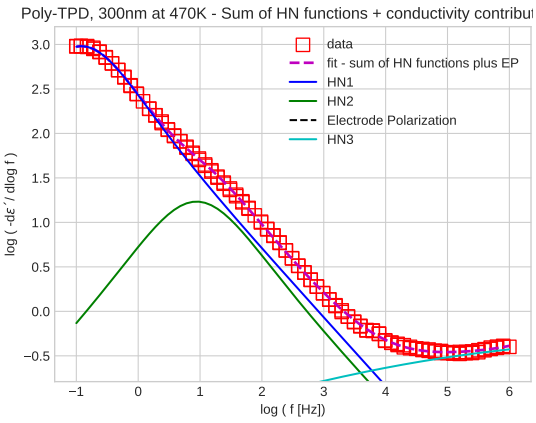

(a) 470K

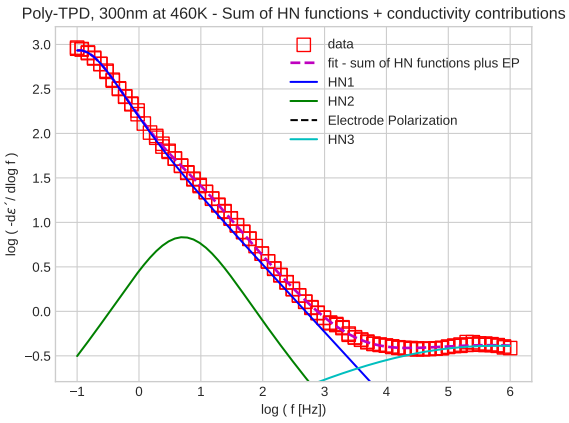

(b) 460K

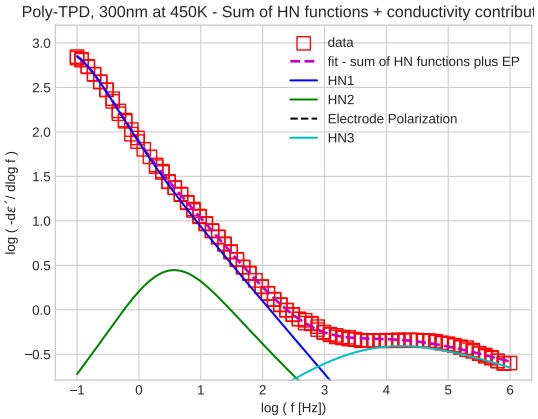

(a) 450K

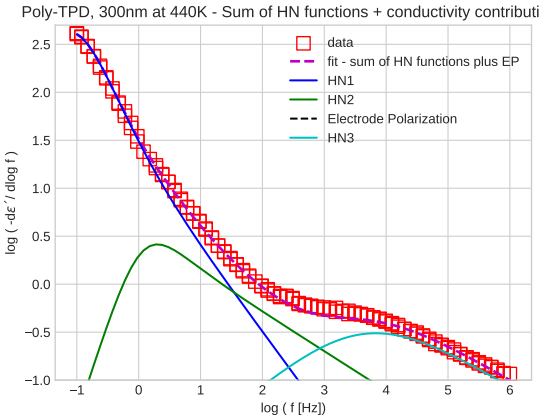

(b) 440K

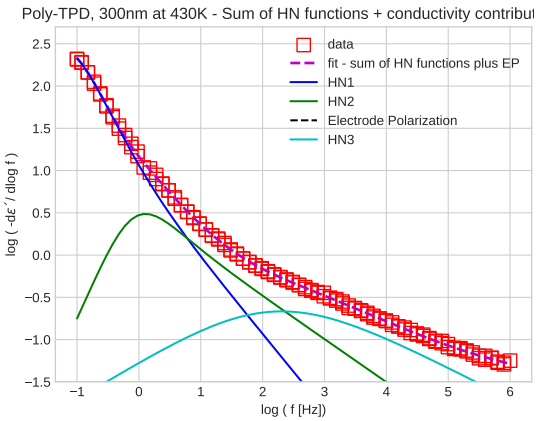

(a) 430K

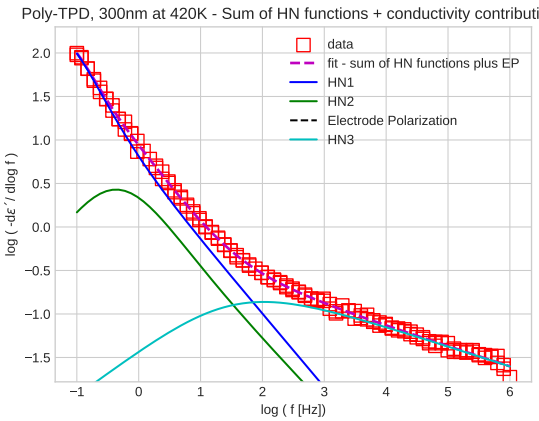

(b) 420K